Space charge effects in photoemission electron microscopy using amplified femtosecond laser pulses

2009 J. Phys.: Condens. Matter 21 314003

(http://iopscience.iop.org/0953-8984/21/31/314003)

J. Phys.: Condens. Matter **21** (2009) 314003 (7pp) doi:10.1088/0953-8984/21/31/314003

Space charge effects in photoemission electron microscopy using amplified femtosecond laser pulses

N M Buckanie, J Göhre, P Zhou, D von der Linde, M Horn-von Hoegen and F-J Meyer zu Heringdorf

Department of Experimental Physics, University Duisburg-Essen, Lotharstrasse 1, D-47057 Duisburg, Germany

E-mail: niemma.buckanie@uni-due.de and meyerzh@uni-due.de

Received 29 December 2008, in final form 5 February 2009
Published 7 July 2009
Online at stacks.iop.org/JPhysCM/21/314003

Abstract

Linear and nonlinear photoemission microscopy is used to study the origin of space charge effects that are frequently observed if amplified femtosecond lasers are used for generation of photoelectrons. Space charge effects are apparent in the width of the photoemission spectra, but also create image blur. The onset threshold for space charge effects is determined by recording the width of photoemission spectra and by finding the conditions under which spectral broadening is just less than the energy resolution of the microscope. The principal findings are independent if harmonics of the fundamental of the fs laser pulses are used, but the space charge effects are found to be more dominant at lower repetition rates. By inserting apertures into the electron path, the place at which space charge effects occur can be localized.

(Some figures in this article are in colour only in the electronic version)

1. Introduction

Photoemission electron microscopy (PEEM) is a versatile technique to study the electronic structure of surfaces. Among other mechanisms, the obtained contrast in PEEM depends on the work function and density of states (DOS) that are accessible by the choice of the light source. While with a conventional Hg discharge lamp only electronic states near the Fermi edge can be studied, UV photoemission using He lamps [1] or UV lasers allows studying of deeper lying electronic states. Finally, synchrotron radiation, with photon energies of several 10 eV, opens the gate into core level spectromicroscopy [2].

During the last few years, the temporal domain has been added to photoemission microscopy [3, 4] due to the availability of ultrashort laser pulses with pulse durations from femtoseconds (fs) to attoseconds (as). The combination of PEEM with fs lasers allows studying of ultrafast processes such as electron–electron dynamics [5] and plasmonics [6]. Several problems are involved, however, when combining ultrashort laser pulses with PEEM. In many cases the photon energy of the pulses is smaller than the work function of the material system of interest. Accordingly, nonlinear photoemission processes are needed, which for many systems are not very effective. One possibility to improve the photoemission yield is then the deposition of Cs to lower the work function of the surface. For instance, after Cs deposition 1PPE processes can be obtained from an Si(001) surface even with a green continuous wave laser ($E_{\hbar\omega} = 2.3$ eV) [7]. A second possibility for improving the photoemission yield is to increase the pulse intensity and reduce the pulse duration to make nonlinear photoemission processes more likely. This can be achieved by ultrashort and ultraintense pulses from femtosecond laser amplifier systems. A third possibility is the generation of harmonics of the fundamental laser pulses to increase the photon energy until threshold photoemission (1PPE) becomes possible. The downside of this approach is the loss of a great portion of the laser intensity due to the low conversion rates. Even worse, amplified fs laser systems work at a lower repetition rate than the 80 MHz of the commonly used Ti:sapphire oscillators and thus compress more photons into fewer pulses by maintaining the same average laser intensity. Such high photon densities result in the emission of a large number of photoelectrons during the

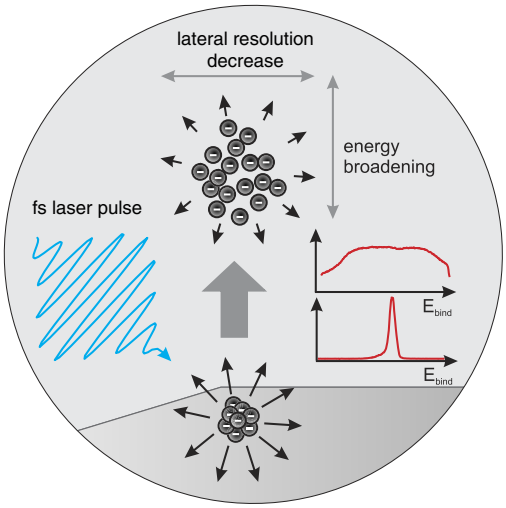

Figure 1. Illustration of space charge effects and their impact on PEEM measurements. The Coulomb repulsion of the photoelectron cloud leads to a broadening of the kinetic energy distribution of the photoelectrons (displayed in the graphs on the right-hand side of the image) and consequently results in image blur.

interaction of the fs pulse with the surface. In addition, the photoelectrons originate only from a small area on the surface, i.e. an area with a size that is defined by the size of the laser spot on the surface. The consequence is space charge effects that affect the energy distribution of the emitted electrons and cause image blur. Figure 1 illustrates the effects of space charge on a propagating electron pulse. The initial energy distribution of the photoelectrons and the high electron density in the pulse cause Coulomb repulsion. As a result, the electron cloud expands energetically as well as laterally [8, 9]. While the expansion of a free propagating electron pulse has already been studied [9], the location at which the most severe Coulomb repulsion takes place in PEEM is still unclear. The energetic broadening could occur immediately at the sample surface, between the sample surface and the objective lens, or further down in the microscope column. For spectromicroscopy space charge has simply to be prevented at all costs, and it is important to know when and where space charge effects occur and how they could be prevented. Here we report on our observation of space charge effects in linear and nonlinear photoemission and discuss the impact that space charges have on PEEM measurements.

2. Experimental set-up

The experiments have been performed in a spectroscopic PEEM from ELMITEC (SPE–PEEM III [12]). The ultrahigh vacuum (UHV) instrument combines photoelectron microscopy with photoelectron spectroscopy by means of an imaging hemispherical energy analyzer. While a detailed description of the electron optics has already been given by Schmidt *et al* [10], we need to emphasize some specific properties of the system. Figure 2 shows a sketch of the main components of the electron optics. The surface is represented by the upright arrow on the left side. The distance between the sample surface and the objective lens is approximately 2 mm and photoemitted electrons are accelerated toward the objective lens by the microscopes bias voltage of 20 kV. The objective lens forms a first focal plane and a roughly 40× magnified image [13]. An aperture is placed in this first image plane (selected-area aperture) to select a region of interest on the surface. The subsequent four lenses in the imaging column, TL to P1, define the overall location of image and diffraction planes in the microscope independently. In RL, the electrons are decelerated to the pass energy of the energy analyzer of $E_{\mathrm{pass}} = 1250$ eV. The system of three lenses following RL summarizes the function of the hemispherical energy analyzer, with the image plane located in the symmetry plane of the

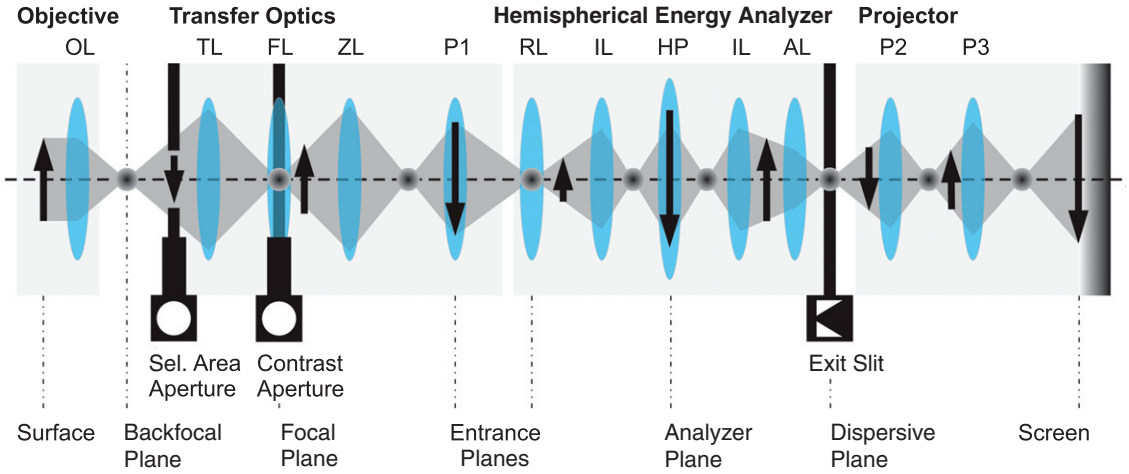

Figure 2. Optical design of the SPE–PEEM III after [10, 11]. The electrons are accelerated by a bias of 20 kV from the surface towards the objective lens. The electrons are decelerated between the transfer optics (TL–P1) before entering the hemispheric analyzer at RL. After passing through the analyzer, the electrons are re-accelerated in AL. The final magnification is obtained by the projector lens system (P2 and P3). Three apertures are available to modify the acceptance angles at different places in the microscope. The selected-area aperture is located in an image plane and is used to select a region of interest on the sample. The contrast aperture is placed in a focal plane. The exit slit of the energy analyzer can be inserted for energy-resolved imaging and angular-resolved photoemission measurements.

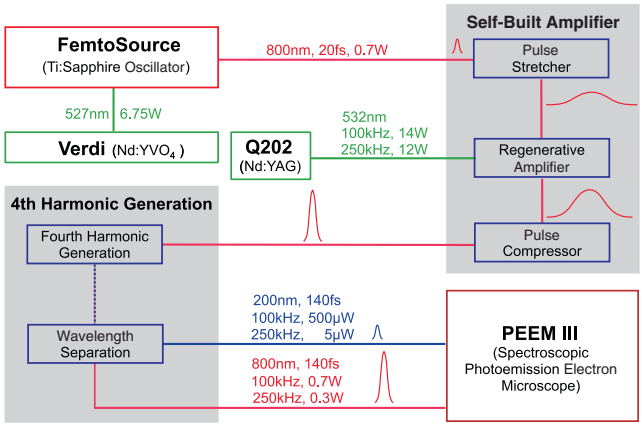

Figure 3. The sketch of the laser set-up used including the home-built amplifier system. The seed pulses are generated by a 80 MHz Ti:sapphire oscillator and pass through the regenerative amplifier. The amplified $\lambda = 800$ nm pulses can then be used to generate the fourth harmonic by passing the fundamental of the laser through a set-up of three BBO crystals.

analyzer. After passing the analyzer, the electrons are re-accelerated by the microscope's bias voltage of 20 kV. The final magnification is achieved by the projection lenses P2 and P3. The focal length of the projection lens P2 can be adjusted to either display the image plane of the analyzer on the screen, or display the energy-dispersive plane of the analyzer, to allow parallel recording of energy spectra over an energy range of $\Delta E \approx 10$ eV.

We use Ag islands that were grown on Si(111). The Si(111) substrates were degassed for several hours at 500 °C and flash annealed to 1200 °C to remove the protective oxide layer. The Ag islands were then formed by self-assembly [14–16] by molecular beam evaporation of Ag from a home-built effusion cell [17, 18] at a substrate temperature of about 600 °C.

Figure 3 gives an overview of the laser set-up used. A home-built regenerative amplifier is seeded by a commercial sub-20 fs pulse duration Ti:sapphire oscillator (FEMTOLASERS GmbH [19]). The amplification is achieved by the technique of chirped pulse amplification [20], and accordingly the amplifier consists of a pulse stretcher, an Nd:YAG pumped regenerative amplifier and a pulse compressor. The amplified femtosecond laser pulses have a pulse duration of about 150 fs and a wavelength of 800 nm ($\hbar\omega = 1.55$ eV). The amplifier is specifically designed for operating at different repetition rates up to 250 kHz. The maximal energy per pulse varies from 1 to 15 μJ, depending on the repetition rate. An additional set-up of 3 BBO crystals is used to generate the fourth harmonic and extends the available photon energy to 6.2 eV. The overlapping different wavelengths are separated with a prism. Finally, the pulses are focused by a lens ($f = 1$ m) and passed through a quartz window into the vacuum chamber. The angle between the laser pulse and the surface normal of the sample is 74°. The spot size on the sample has a diameter of about 200 μm $\times$ 400 μm (FWHM) for the $\lambda = 800$ nm fundamental and about 400 μm $\times$ 1450 μm (FWHM) for the fourth harmonics.

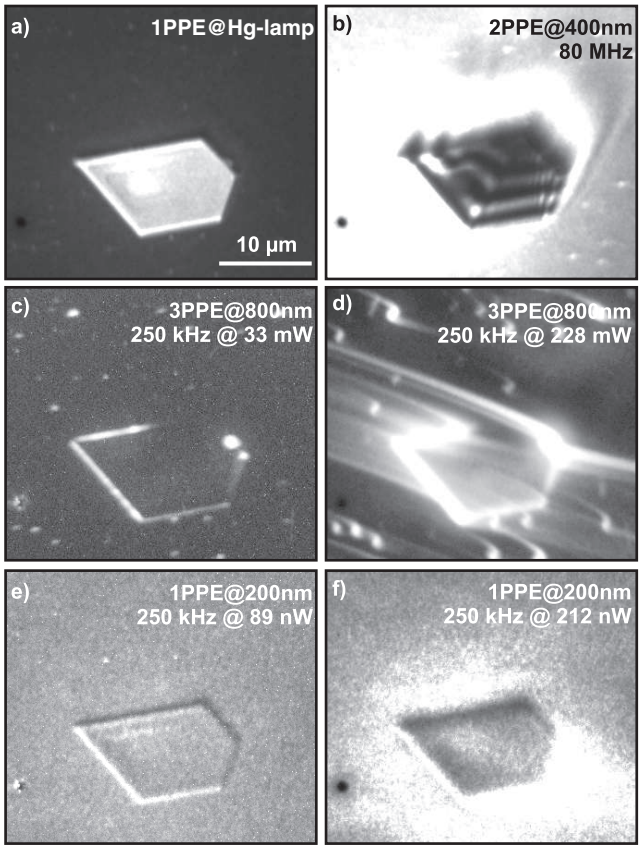

Figure 4. PEEM images of the same Ag island recorded using different illumination sources. (a) Conventional Hg lamp. (b) Second harmonic ($\lambda = 400$ nm) of the Ti:sapphire oscillator (c) and (d) fundamental ($\lambda = 800$ nm) of the femtosecond amplifier at two different laser intensities. (e) and (f) Fourth harmonic ($\lambda = 200$ nm) of the femtosecond amplifier at two different laser intensities.

3. Results and discussion

Figure 4 shows PEEM images of the same silver island recorded under illumination with different light sources. Panel (a) has been recorded with the Hg discharge lamp and shows the topography of the Ag island on the Si(111) substrate. No space charge effects are visible in this 1PPE image. In panel (b), the use of frequency-doubled $\lambda = 400$ nm laser pulses from the Ti:sapphire oscillator causes nonlinear 2PPE to become the dominating process of the photoelectron generation. The bright features on top of the Ag island in panel (b) originate from surface plasmon polaritons (SPP) in the Ag island [6, 21]. As in panel (a), no space charge effects are present in the image.

The remaining panels (c)–(f) of figure 4 were recorded using amplified laser pulses at a repetition rate of 250 kHz. In panels (c) and (d) we used the $\lambda = 800$ nm fundamental of the amplifier system at two different laser intensities. At the lower intensity (c) the image appears focused with no apparent contrast between the Ag island and the Si background. Only the edges of the island and some hot-spots [3, 22] produce contrast. At a higher laser intensity, panel (d) of figure 4, the contrast is similar to panel (c), but the image is severely

distorted. To compare the nonlinear photoemission (3PPE for $\lambda = 800$ nm laser pulses) with threshold photoemission (1PPE), figures 4(e) and (f) show PEEM images under illumination with the ($\lambda = 200$ nm) fourth harmonic of the amplified laser pulses. Again, under illumination with a low intensity in panel (e) the contrast between the island and the surrounding is weak. The edges of the island appear bright at the front due to field enhancement effects, while shadowing causes the backside of the island to appear dark. The hot-spots from panel (c) and (d) are not visible any more. At the higher laser intensity, panel (f), the contrast is similar as in panel (e), but the island—under the same microscope settings as in panel (e)—appears blurred.

Apparently, higher laser peak intensities, panels (d) and (f), result in blurred or severely distorted images. We will in the following discuss the image blurring and the broadening of the energy spectra for the two wavelengths (800 and 200 nm) independently, using spatially resolved photoemission spectroscopy in the PEEM to determine the origin of these effects.

3.1. 800 nm laser pulses

Figure 5 shows energy spectra of an area on the surface that contains a hot-spot. The spectra were recorded in the dispersive plane mode of the microscope at different laser intensities without (a) and with ((b) and (c)) a contrast aperture of a diameter of 50 μm. All red solid curves in figure 5 were recorded using 800 nm laser pulses, the green dashed curves were recorded with the Hg discharge lamp ($\hbar\omega_{\max} = 4.9$ eV) and represent the expected 1PPE spectrum for the given microscope settings. The 'Gaussian' appearance of the spectrum is caused by the small accessible energy range ($E_{\mathrm{Hg-lamp}} - \Phi_{\mathrm{Ag}} \approx 0.65$ eV) and the convolution of the expected narrow spectrum with the energy resolution function of the microscope ($\Delta E = 230$ meV). Panel (a) of figure 5 displays several energy spectra of the hot-spots at average laser intensities from 100 mW (top) to 10 mW (bottom). The energy spectra at higher laser intensities exhibit a much larger width than the spectrum that was obtained with the Hg discharge lamp. When the laser intensity is reduced, the width of the spectra decreases. The laser power, at which the width of the energy spectra does not decrease further, defines a power threshold below which space–charge-related energy broadening is smaller than the energy resolution of the microscope.

To determine where the space charge effect occurs, we inserted a 50 μm diameter contrast aperture into the beam and repeated the experiment. The results for different laser intensities are displayed in the bottom panels of figure 5 for higher laser fluences (b) and for lower laser fluences (c).

Interestingly, insertion of the contrast aperture reduces the energy broadening drastically, and the measurements with and without contrast aperture suggest that space charge effects evolve somewhere between the contrast aperture and the exit slit of the analyzer. Since the electron density in the focal planes of all lenses in the electron optical column is lower than the electron density in the back focal plane of the objective

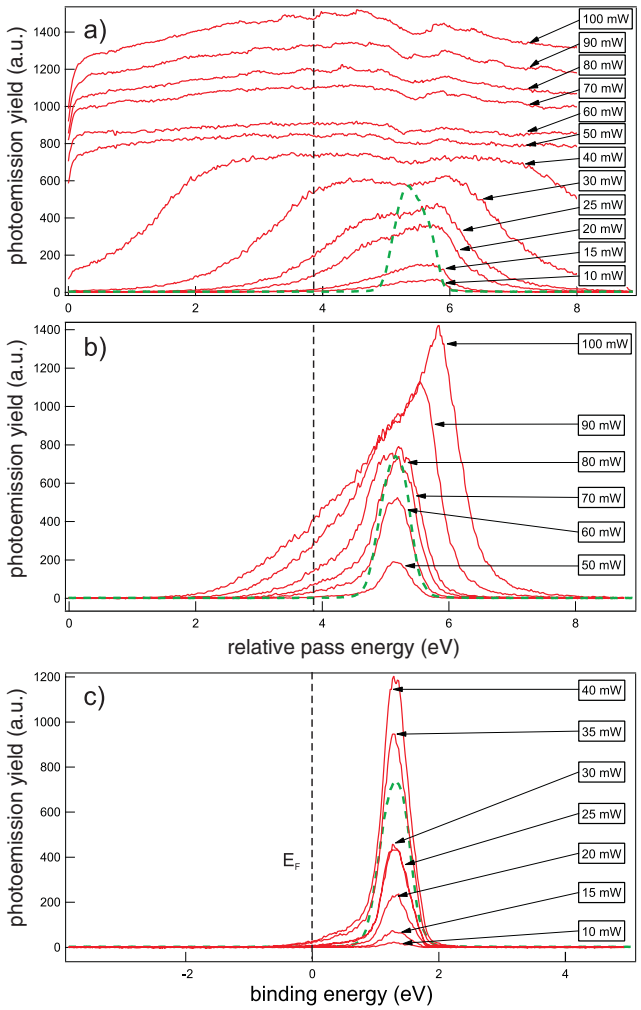

Figure 5. Energy spectra of photoelectrons as a function of the average laser power (marked with arrows) for 800 nm laser pulses of the amplifier system at a repetition rate of 100 kHz. The dashed green curves represent energy spectra that have been obtained with the Hg lamp under the same imaging conditions. (a) Without contrast aperture; (b) with 50 μm contrast aperture. The space charge effect is significantly reduced. (c) Same as in (b), but for lower laser intensities.

lens, we do not expect additional space charge effects from the two lenses P2 and P3 of the projection system. The same argument applies to the four lenses in the transfer optics between the selected-area aperture and the entrance of the analyzer. The most likely candidate where space charge effects could occur is the retarding lens RL, because here the electrons are decelerated. This deceleration results in an accumulation of electrons in the focal plane of RL and, hence, the Coulomb repulsion has a much stronger effect, i.e. the space charge broadening will be most prominent here.

To avoid space charge artifacts, it is necessary to determine the critical laser fluence threshold below which the PEEM images are not affected by the Coulomb repulsion. Although the shape of the spectra changes as a function of the laser intensity, we simply determine the full width at half-maximum (FWHM) of the spectra to compare the different spectra. Figure 6 shows the FWHM of the energy spectra

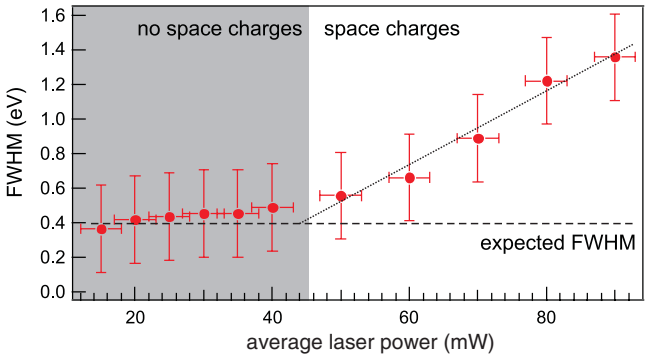

Figure 6. The spectral width of the energy curves in figures 5(b) and (c) as a function of the average laser power. The laser pulses used have a wavelength of 800 nm with a repetition rate of 100 kHz. The dashed line represents the expected width of the energy spectra without any space charge effects present. The dotted line is a guide to the eye. The error bars in the x direction represent the uncertainty in the determination of the laser power due to power meter error ($\Delta \approx \pm 2$ mW). The error bars in the y direction are due to 0.23 eV the energy resolution of the PEEM.

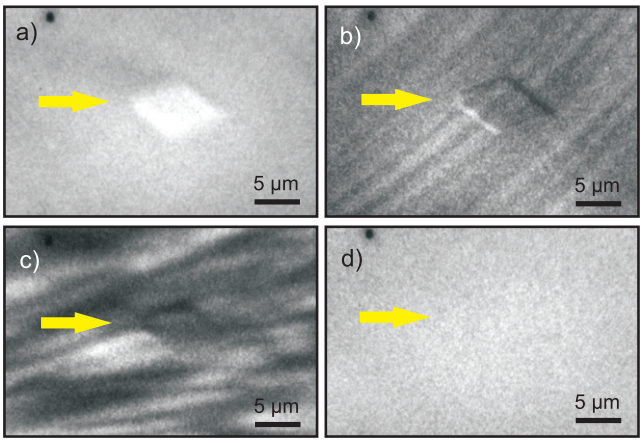

Figure 7. Extreme space charge effects during illumination of the surface with unattenuated 200 nm laser pulses at 250 kHz repetition rate. The yellow arrows mark the position of the island in each image. Space charge effects cause the edges of the island to appear blurred. Slight changes in the laser spot position on the sample result in contrast inversion ((a) and (b)) and even a complete loss of contrast ((c) and (d)) can be achieved.

from figures 5(b) and (c) as a function of the average laser intensity. Again, a trend can be recognized that higher laser intensity results in a more pronounced space charge effect. Below an average laser power of ≈45 mW, however, the width of the energy spectra does not change any more. This threshold accords to a maximum pulse intensity of 4×10^9 W cm^{-2}. The corresponding width is shown as a dashed line in figure 6. Considering the photon energy of $E_{\hbar\omega} = 1.55$ eV, the Ag work function of $\Phi = 4.25$ eV [23, 24] and that a 3PPE process is necessary for photoemission, one arrives at an expected width of the energy spectrum of $3E_{\hbar\omega} - \Phi = 0.4$ eV, which agrees well with the observation and is slightly smaller than the expected value of Hg lamp spectral width ($\Delta E_{\mathrm{Hg-lamp}} = 0.65$ eV).

3.2. 200 nm laser pulses

To compare the above results for 3PPE with 1PPE, the fourth harmonic of the fs laser pulses was generated and coupled into the PEEM.

Figure 7 shows four images of the same Ag island recorded during an experiment with high laser intensity, where in each panel the position of the laser spot on the sample surface was slightly changed. This slight change in the illumination, however, had a dominating impact on the obtained contrast. While in figure 7(a) the island appears bright and no proper focusing is possible, the island appears darker than the surrounding area ((b), (c)), and finally (d) the island is not visible at all. Additionally, there are periodic intensity variations that vary with the laser position on the surface that are also attributed to space charge effects. Energy spectra for the different situations in figure 7 easily yield a width of 20 eV.

Finally we again determine the threshold laser power below which the energy broadening of the spectra is negligible. The data of this experiment are shown in figure 8(a), where again the width of the energy spectra decreases with reduced laser power. Plotting the widths of the energy spectra as a function of the average laser power, figure 8(b), we determine the threshold for the onset of significant space charges to be 4×10^7 W cm^{-2}.

4. Conclusion

We studied the space charge effects in PEEM using fs laser pulses of different photon energies, i.e. exploited linear and nonlinear photoemission processes. When the fs laser amplifier was used, in both cases it was possible to drive the system into the space–charge-limited regime. We find that at the onset of significant space charge effects a broadening of the energy spectra occurs. For the 200 nm laser pulses the critical threshold for the observation of space charge effects is about 4×10^7 W cm^{-2}, approximately 100 times smaller than for the 3PPE case with 800 nm laser pulses, 4×10^9 W cm^{-2}. We believe the space charge to occur in the RL lens of the electron column, rather than between the sample surface and the objective lens. This finding is fundamentally different from the case of ultrafast electron diffraction [25, 26], where space charge broadening of the electron distribution occurs during the free propagation of the electron pulse through vacuum. Our observation that in PEEM the electron optical elements are, to a large extent, responsible for the space charge effect is supported by the observation that a reduction of the electron density in the column by reduced the space charge broadening, while the electron density in the back focal plane of the objective lens was not affected by the presence of the contrast aperture. At even higher laser intensities, the spatial resolution is lost, and all features turn into elongated lines that extend over the entire field of view, or cause such significant image blur that a featureless image results. Considering the enormous energy spread that can be caused by the space charge effect, it is not surprising that the elongations occur in the dispersive direction of the hemispherical energy analyzer. Figure 5 shows energy

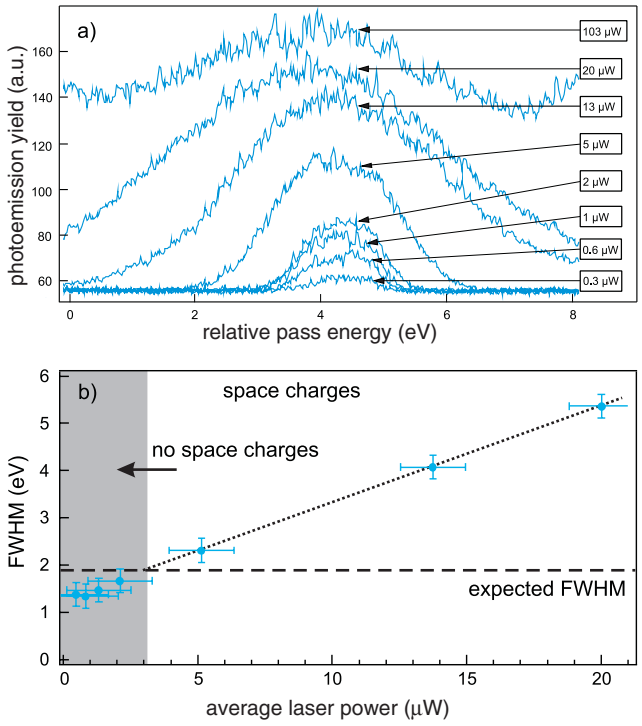

Figure 8. (a) Energy spectra of photoelectrons as a function of the average laser power using 200 nm laser pulses. The width of the energy spectra decreases during the reduction of the average laser power. This experiment is analogous to the experiment in figure 5. (b) The dependence of spectral widths on the laser power used. The threshold power below which space charge effects become negligible is marked by the gray rectangle. The dotted line represents a guide to the eye. The dashed line marks the expected width of the energy curves from panel (a).

spectra, at higher laser fluence, that span the whole accessible energy range of the dispersive plane imaging mode. In these cases, the energy spread will be tens of eV. We believe that the energy spread in these cases is so large that the different electron paths in the analyzer do not overlap any longer. For regular energy filtered imaging this is not an issue, as the pass energy of the electrons is adjusted by the start voltage of the microscope. Even for electron clouds with a large electron energy spread, for instance created by synchrotron light, the electrons that pass through the analyzer slit will always have the same relative energy. These electrons will take the same path through the analyzer and will, in all cases, provide a sharp image. For PEEM in the space-charge-limited regime, in contrast, the electron cloud gets disturbed while propagating through the microscope, with a negative impact on the imaging properties.

Apparently, the only way to eliminate space charge effects is to reduce the average laser power. This procedure is essential for studying the electronic properties of nanostructures with fs laser pulses and will require the construction of amplifier systems with high repetition rates in order to minimize exposure times. In the first experiments that we performed with an amplifier system that had a repetition rate of 1 kHz, the space charge effects were so dominant that recording of spectra in the dispersive plane mode of the microscope below the onset threshold for space charges required exposure times of more than 15 min per spectrum. Energy-filtered imaging under such conditions is almost impossible. In contrast, as we have shown here, repetition rates of 100 kHz and more are suitable for energy-filtered spectromicroscopy without significant space charges. With increasing repetition rates of new amplified fs laser systems, we expect space charge effects to be less and less of an issue.

Acknowledgments

Financial support of the Deutsche Forschungsgemeinschaft in the program SFB 616 'Energy Dissipation at Surfaces' is gratefully appreciated. We would like to acknowledge fruitful discussions with the ELMITEC team.

References

[1] Tromp R 2008 *EMC2008: Proc. 14th European Microscopy Congress* vol 1 *Instrumentation and Methods* p 735
[2] Meyer zu Heringdorf F-J, Schmidt T, Heun S, Hild R, Zahl P, Ressel B, Bauer E and Horn-von Hoegen M 2001 *Phys. Rev. Lett.* **86** 5088
[3] Schmidt O, Bauer M, Wiemann C, Porath R, Scharte M, Andreyev O, Schönhense G and Aeschlimann M 2002 *Appl. Phys.* B **74** 223
[4] Meyer zu Heringdorf F-J, Chelaru L, Möllenbeck S, Thien D and Horn von Hoegen M 2007 *Surf. Sci.* **601** 4700
[5] Bayer D, Wiemann C, Gaier O, Bauer M and Aeschlimann M 2008 *J. Nanomater.* **2008** 249514
[6] Chelaru L I and Meyer zu Heringdorf F-J 2007 *eCOSS-24: Proc. 24th European Conf. on Surface Science*; *Surf. Sci.* **601** 4541
[7] Thien D, Kury P, Horn-von Hoegen M, Meyer zu Heringdorf F-J, van Heys J, Lindenblatt M and Pehlke E 2007 *Phys. Rev. Lett.* **99** 196102
[8] Knauer W 1979 *J. Vac. Sci. Technol.* **16** 1676
[9] Siwick B J, Dwyer J R, Jordan R E and Miller R J D 2002 *J. Appl. Phys.* **92** 1643
[10] Schmidt T, Heun S, Slezak J, Diaz J, Prince K, Lilienkamp G and Bauer E 1998 *Sur. Rev. Lett.* **5** 1287
[11] ELMITEC *Manual PEEM III*
[12] ELMITEC Elmitec home page http://www.elmitec.de/ 07 Dec. 2008
[13] Elmitec, personal communication
[14] Naitoh M, Shoji F and Oura K 1991 *Surf. Sci.* **242** 152
[15] Zhang Z H, Hasegawa S and Ino S 1997 *Phys. Rev.* B **55** 9983
[16] Lijadi M, Iwashige H and Ichimiya A 1996 *Surf. Sci.* **357/358** 51
[17] Kury P, Hild R, Thien D, Gunter H-L, zu Heringdorf F-J M and von Hoegen M H 2005 *Rev. Sci. Instrum.* **76** 083906
[18] Meyer zu Heringdorf F-J and Belton A 2004 *Rev. Sci. Instrum.* **75** 5288
[19] Femtolasers-GmbH *Femtosecond Technology* http://www.femtolasers.com 31 Oct 2006
[20] Strickland D and Mourou G 1985 *Opt. Commun.* **55** 447
[21] Kubo A, Pontius N and Petek H 2007 *Nano Lett.* **7** 470
[22] Cinchetti M, Valdaitsev D A, Gloskovskii A, Oelsner A, Nepijko S A and Schönhense G 2004 *iCESS-9: Proc. 9th*

Int. Conf. on Electronic Spectroscopy and Structure; *J. Electron Spectrosc. Relat. Phenom.* **137–140** 249
[23] Michaelson H B 1977 *J. Appl. Phys.* **48** 4729
[24] Halas S and Durakiewicz T 1998 *J. Phys.: Condens. Matter* **10** 10815
[25] Janzen A, Krenzer B, Zhou P, von der Linde D and von Hoegen M H 2006 *Proc. 23rd European Conf. on Surface Science (Berlin, Sept. 2005)*; *Surf. Sci.* **600** 4094
[26] Siwick B J, Dwyer J R, Jordan R E and Miller R J D 2003 *Science* **21** 1382